RESEARCH ARTICLE

Unravelling the puzzle of anthranoids metabolism in living plant cells using spectral imaging coupled to mass spectrometry

Quentin Chevalier[a,b,1], Jean-Baptiste Gallé[a], Nicolas Wasser[a], Valérie Mazan[c], Claire Villette[b], Jérôme Mutterer[b], Maria M. Elustondo[d], Nicolas Girard[a], Mourad Elhabiri[c], Hubert Schaller[b], Andréa Hemmerlin[b], Catherine Vonthron-Sénécheau[a]

[a] Laboratoire d'Innovation thérapeutique, Centre National de la Recherche Scientifique-Université de Strasbourg, Illkirch, France, F-67401 Cedex

[b] Institut de Biologie Moléculaire des Plantes, Centre National de la Recherche Scientifique-Université de Strasbourg, Strasbourg, France, F-67084 Cedex

[c] Laboratoire d'Innovation Moléculaire et Applications, Centre National de la Recherche Scientifique-Université de Strasbourg-Université de Haute Alsace, Strasbourg, France, F-67087 Cedex

[d] SUPINFO École des Experts des Métiers de l'Informatique, Strasbourg, France, F-67004 Cedex

[1] Address correspondence to qchevalier67@gmail.com

Short title: Anthranoids Metabolism

The author(s) responsible for distribution of materials integral to the findings presented in this article in accordance with the policy described in the Instructions for Authors (www.plantcell.org) is: Quentin Chevalier (qchevalier67@gmail.com)

Abstract

Vismione H (VH) is a fluorescent prenylated anthranoid produced by plants from the Hypericaceae family, with antiprotozoal activities against malaria and leishmaniosis. Little is known about its biosynthesis and metabolism in plants or its mode of action against parasites. When VH is isolated from *Psorospermum glaberrimum*, it is rapidly converted into madagascine anthrone and anthraquinone, which are characterized by markedly different fluorescent properties. To locate the fluorescence of VH in living plant cells and discriminate it from that of the other metabolites, an original strategy combining spectral imaging (SImaging), confocal microscopy and non-targeted metabolomics using mass spectrometry, was developed. Besides VH, structurally related molecules including madagascine, emodin, quinizarin as well as lapachol and fraxetin were analyzed. This strategy readily allowed a spatiotemporal characterization and discrimination of spectral fingerprints from anthranoids-derived metabolites and related complexes with cations and proteins. In addition, our study validates the capability of plant cells to metabolize VH into madagascine anthrone, anthraquinones and unexpected metabolites, leading to new hypotheses on the metabolism of anthranoids in plants.

INTRODUCTION

The plant kingdom is a source of ~200.000 identified specialized metabolites of which, ~10.000 are phenolic compounds also called polyphenols. Many of these metabolites are used as ingredients in the pharmaceutical, cosmetics and agri-food industries on account of their diverse bioactive properties (Tissier et al., 2014). Anthranoids form a large class of polyphenols including anthraquinones, anthrones and bianthrones characterized by anthracene-based structures with various degree of oxidations and conjugated with sugars and/or prenyl groups (Mazimba et al., 2013). The biological action of well-studied anthraquinones requires specific structural groups. For instance, in the case of emodin (emo), hydroxyl groups at position 1 and 8 of the anthracene ring (Figure 1A) are mandatory for its purgative properties (Dong et al., 2016; Srinivas et al., 2007).

Vismione H (VH) (Figure 1A) is a prenylated anthranoid, generating significant interest due to promising antimalarial and antileishmanial activities (François et al., 1999; Gallé, 2015). Chemical inventories of botanical resources, structural elucidation and biological activities of natural products like VH allowed a compilation of comprehensive repositories for potential drugs. Still, fundamental questions about their biosynthesis *in planta*, their molecular targets for biological activities and their metabolization in cells into potentially active derivatives remain unsolved.

In plants, anthranoids are biosynthesized through two distinct pathways: the polyketide pathway occurs in the Rhamnaceae, Fabaceae, Aloeaceae, Polygonaceae families, while the shikimate/*o*-succinylbenzoic acid pathway in Rubiaceae (Han et al., 2001). Recently, genome mining identified new candidates for anthraquinones biosynthesis enzymes in *Senna tora* plants (Kang et al., 2020). Anthranoid metabolism has also been reported in mushrooms belonging the *Cortinarius* genus and in *Aspergillus nidulans* (Gill, 2001; Chiang et al., 2010). These data suggest that O-methylation, oxidation, hydroxylation, dimerization, glycosylation may be enzyme-catalyzed, while other modifications could result from chemical reactions such as tautomerization, photoisomerization and photochemical hydroxylation (Fain et al., 2006; Furumoto and Jindai, 2008; Elkazaz and Jones, 2010). Under oxidative conditions like in DMSO, the VH isolated from *Psorospermum glaberrimum* spontaneously degrades into anthrone form, which is then oxidized into its madagascine (Mad) anthraquinone form or alternatively dimerized into bianthrones (Gallé, 2015).

Within the entire UV-Vis. spectrum, more than 300 naturally occurring fluorescent compounds have been reported with quantum yields ranging from 0.01% to 100% *in vitro* (Duval and Duplais, 2017). Anthranoids exhibit distinct fluorescence properties in spite of their chemical structure similarities, this allowing their differentiation by spectral analysis. In fact, the number and position of substituents, especially hydroxyl groups impact the physico-chemical (*i.e.,* protonation) and fluorescence properties of anthranoids (Duval and Duplais, 2017). The acetyl vismione D emits green fluorescence (λ_{Em} = 534 nm) in

methanol with a low quantum yield of about 2% (Gallé, 2015), whereas anthrones/anthranols emit light at a blue wavelength (λ_{Em} = 458 nm) in alcohols and a strong yellow-green fluorescence in water (λ_{Em} = 539 nm) (Fujii et al., 1997). In regards to anthraquinones such as quinizarin (Qui) (Figure 1A) or hypericin, both fluoresce in the orange to far red window (570-675 nm) with quantum yield up to 30 % (Fujii et al., 1997; Rossi et al., 2010; Verebova et al., 2016; Duval and Duplais, 2017). Overall, the specific fluorescence properties of VH, anthrone and anthraquinone forms have never been exploited in integrative biochemical approaches, especially to elucidate their biosynthesis, metabolism, cell compartmentation and bioactivity in living cells.

Spectral imaging (SImaging) enables the simultaneous detection of emitted fluorescence in multiple independent channels with a resolution < 10 nm/channel (Figure 1B). Auto-fluorescent phenolic compounds such as simple phenols, vanillin and mangiferin were observed by SImaging indeed (Conéjéro et al., 2014; Talamond et al., 2015). Here, SImaging combined with high-resolution mass spectrometry was implemented to track VH, related anthranoids (Mad, Emo, Qui) and compared to a prenylated naphthoquinone lapachol (Lap) in tobacco BY-2 cells (Figure 1A and 1B). Tobacco cells were chosen as a model because it is inexpensive, safe, easy to handle and free of auto-fluorescent compounds under standard conditions (Nagata et al., 1992). Fraxetin (Fra) was used as a positive control because its fluorescence and metabolism are reported in *Arabidopsis* and tobacco BY-2 cells (Tsai et al., 2018; Lefèvre et al., 2018). To faithfully characterize the molecules on the basis of their fluorescence observed by SImaging, we performed a spectrofluorometric analysis of pure compounds in solution as a reference (Figure 1B). This comparison allowed for the identification of natural products fluorescence signals within different cell compartments at a single time point. Combined with non-targeted metabolomics (*UPLC-HRMS/MS*) of treated tobacco cells, providing unique and accurate annotations of fluorescent metabolites (Figure 1C), this elegant photobiochemistry approach offer a fresh eye on the fate of the antimalarial agent vismione H in living plant cells.

RESULTS

pH influences the spectral properties of compounds in solution.

pH values and composition in salts differ in plant sub-cellular compartments, hinging on cell type, the developmental stage and environment (Binzel et al., 1988; Carden et al., 2003). As the intracellular pH in plant cells ranges from 5 in the primary vacuole, up to 8 in the mitochondrial matrix and peroxisomes (Shen et al., 2013; Martinière et al., 2013), we have investigated in detail the photophysical properties of anthranoids and coumarins, whose fluorescence is under physiochemical control. It is noteworthy that all studied compounds showed at least two main absorption bands, one with high absorptivity at wavelengths below 300-320 nm and another less intense band at much lower energies (from 350-600 nm, see Supplemental Figure S1 and Table S1). In all examined systems, a significant bathochromic shift of the absorption lying at lower energies was observed upon increasing pH. In contrast, a hypochromic shift of the main absorption band and the emergence of a weak absorption band, centered at about 500 nm under basic conditions, was observed for VH (see Supplemental Figure S1A to S1C). As reported for other polyphenols (Friedman and Jürgens, 2000; Giusti and Wrolstad, 2001), these results showcase the impact of the moderate acidity and the associated hydroxyl deprotonation of the investigated polyphenols on their respective absorption spectral characteristics. In addition, the second absorption centered at 350-600 nm is appropriate to SImaging methodology settings and to those of most confocal microscopes.

Among the six compounds studied, with the exception of Lap (see Supplemental Figure S2F), all compounds emitted fluorescence when excited between 350-520 nm (Figure 2). In an organic solvent such as ethyl acetate, VH did not emit fluorescence as compared to anthraquinones (see Supplemental Figure S2A to S2D), whereas Fra could only be excited by λ < 330 nm (see Supplemental Figure S2E). Still, in saline ethanolic solution at pH 2 (*i.e.,* fully protonated and neutral species), VH and anthraquinones were found to be fluorescent and their absolute quantum yields Φ_F ranged from 0.4 to 15.1% (Table 1, Figure 2A to 2E). Surprisingly, although Mad only differs from the Emo by the prenylated C3-OH

group (Figure 1A), its absolute quantum yield Φ_F = 4.8% was found to be 10 times higher than that of Emo Φ_F = 0.4%. The 1,4-dihydroxyanthraquinone Qui was found to be the most fluorescent anthraquinone with a Φ_F = 15.1%. These results indicate that the number and position of hydroxyl groups as well as other types of substitutions (*e.g.*, prenyl group on position 3 for Mad) on anthraquinones contribute to the brightness of their fluorescence emission. In addition, anthraquinones show a drastic loss of their fluorescence emission intensity (see Supplemental Figure S2B to S2D) when the pH value is higher than the pK_{a1} (*i.e.*, monodeprotonated species, see Supplemental Table S1), and *vice versa* for Fra or VH (catechol for Fra or naphthalene-1,8-diol for VH, see Supplemental Figure S2A and S2E). Nonetheless, subsequent increase of pH to 12 and higher lead to the progressive loss of Fra and VH fluorescence (see Supplemental Figure S2A and S2E). It can be speculated that the former likely promoted VH and Fra degradation into other compounds by lactone ring opening or anthraquinone formation from VH as previously described in DMSO (Hlasiwetz and Grabowski, 1867; Cameron et al., 1976; Gallé, 2015). Interestingly, the λ_{Em} measured for VH in NH_4HCO_3 and $Na_2B_4O_7$ buffers at pH 10 were found to be bathochromically shifted from 481 to 532 nm (LNH_4^+ Φ_F = 23.9%) and 533 nm (LB Φ_F = 31%), respectively (Table 1, Figure 2B, see Supplemental Figure S3A). With $Na_2B_4O_7$ buffer, VH is therefore strongly emitting as reported for anthranol in the Schouteten reaction with $Na_2B_4O_7$ (Fujii et al., 1997). Similarly, Fra λ_{Em} was 492 nm (LB Φ_F = 1.1%) and 481 nm (LNH_4^+ Φ_F = 7.7%) in NH_4HCO_3 (Table 1, Figure 2F, see Supplemental Figure S3B). These results indicate that in cellular environments with acidity ranging from 4 to 7.8, all compounds except Lap and Fra would emit fluorescence if excited at λ_{Ex} ranging from 392 to 480 nm. As far as Fra and VH are concerned, the distinct photophysical properties of the LB and LNH_4^+ characterized species support the fact that these two compounds are likely able to chelate boron as already reported for Mg^{2+} or Fe^{2+} with Fra and anthraquinones (Sedaira et al., 1998; Tsai et al., 2018), but also ammonium. In this context, we have carefully investigated the influence of metals (Ca^{2+} and Mg^{2+}) and the BSA model protein chelation on the VH emission properties.

Metal and protein chelations influence VH fluorescence properties.

Ca^{2+} and Mg^{2+} were selected for complexation studies not only because of their abundance in plant cells, but also for their key roles in cell structure and physiology such as signaling pathways or the water splitting complex of photosystems (Hepler, 2005; Waters, 2011; Guo et al., 2015). BSA was selected as a protein model as it has already been used for protein chelation assays with other fluorescent compounds (Duval et al., 2020). Thus, we evaluated the absorption (26 µM VH) and fluorescence (2.6 µM VH) properties of VH in EtOH/water 1:1 *v/v* containing 0.1 M of NaCl in the presence of Mg^{2+} or Ca^{2+}. As BSA precipitated under these experimental conditions, the protein complexation studies were performed only in water. Accordingly, VH chelates both Mg^{2+} and Ca^{2+} with a comparable affinity (Figure 3, see Supplemental Figure S4 and Figure S5). From the UV-Vis. absorption titrations, log K_{VHM} values of 2.31 $\pm$ 0.07 and 2.24 $\pm$ 0.06 respectively, were calculated and indicated that substantial amounts of VH-Ca or VH-Mg complexes can be formed within the cells. In both cases, about 70% of VH (26 µM) complexation was achieved with 6 mM of $CaCl_2$ or $MgCl_2$. Although VH displays similar binding strength with these metal ions, the absorption data pointed out different binding modes (see Supplemental Figure S4 and Figure S5). Marked spectral differences observed in the case of Ca^{2+} as compared to Mg^{2+} assert divergent coordination preferences. As reported, carboxylates preferentially act as bidentate binders with Ca^{2+} and as monodentate ligands with Mg^{2+} in proteins (Dudev and Lim, 2004). This property could explain our absorption data with VH acting as bidentate ligand with Ca^{2+} (β-hydroxy-ketone binding unit leading, see Supplemental Figure S1A and S1B), while preferentially coordinating Mg^{2+} with monodentate binding unit mode (phenolate unit). Fluorescence analysis of VH-Ca and VH-Mg complexes in solution confirmed the impact of chelation on photophysical properties. The maximum of emission λ_{Em} for VH-Ca and VH-Mg (549 ±1 nm) complexes was found to be higher than that of the VH LB or LNH_4^+ species (532 ±1 nm) (Table 1). Nonetheless, the Φ_F of VH-Ca (19.8%) and VH-Mg (18.6%) complexes were

substantially lower than that of VH LB (31%) species, but still much higher than the neutral species (3.7% for VH LH_2).

We then evaluated the binding strength of VH and Fra with the BSA protein model, both by absorption and emission means (see Supplemental Figure S6A, S6B, S6E and S6F). VH and Fra were found to strongly interact with BSA, with stability constants log $K_{VH\text{-}BSA}$ and log $K_{Fra\text{-}BSA}$ values of 5.3 ± 0.2 and 5.7 ± 0.3 (see Supplemental Figure S7), respectively. This suggests that VH and Fra would interact mainly with proteins rather than with divalent metal ions *in cellula*. VH chelates BSA protein with a weak alteration of the absorption properties as seen previously with Mg^{2+} (Figure 3B, see Supplemental Figure S7A and S7B), while the absorption properties of Fra were significantly altered (see Supplemental Figure S7E and S7F). The λ_{Em} of VH LBSA fluorescence spectrum corresponded to 517 nm with Φ_F = 23.5%, close to that of VH LNH_4^+ species (Table 1, see Supplemental Figure S3C). Similar results were found with Fra-BSA (Table 1, see Supplemental Figure S3D, Figure S6F and S6G). It can be proposed that electrostatic interactions with ammonium residues such as those found in lysine or arginine, allows complexation of VH and Fra with proteins. In contrast, Emo and Qui emissions were almost unaffected in the presence of BSA (see Supplemental Figure S6C, S6D, S6G and 6H), as reported for complexes with DNA (Verebova et al., 2016). Overall, although neutral VH and Fra LH_2 with low Φ_F seemingly predominate at intracellular pH, our results suggest that interactions with endogenous metal ions or proteins might improve/modulate their fluorescence properties *in cellula.*

Fluorescent anthranoids metabolization and transport *in cellula* by spectral imaging. To characterize the fluorescence *in cellula*, we compared the reference emission spectra obtained from our spectrofluorimetric analysis to those measured by SImaging in solution and in living BY-2 cells. SImaging methods were used to discriminate mixed fluorescent signals from the studied compounds in solution and in BY-2 cells with a special focus on vismione H (blue to green-yellowish emission) and related anthraquinones (yellow to red emission) (Figure

1A). With respect to the photophysical data, two different settings have been selected for the excitation and detection of fluorescence using SImaging: λ_{Ex} = 405 nm (λ_{405}) with emission spectra range from 415 to 664 nm, and λ_{Ex} = 488 nm (λ_{488}) with emission spectra range from 495 to 664 nm. The fluorescence data obtained by SImaging on pure compounds in solution at λ_{405} and λ_{488} fit well with those obtained by the spectrofluorimetric approach (Figure 2 and Figure 3, see Supplemental Figure S3). However, some variations can be observed such as a decrease in the intensity of the shoulder of the Emo LH_3 at 575 nm or a shift from 484 to 503 nm for the VH LH_2 or from 492 to 521 nm for the Fra LB. These discrepancies could be related to differences in resolution, glass support or optical path between SImaging (9 nm, glass microscope slide, 1 mm) and spectrofluorimetry (1 nm, quartz cell, 1 cm). In addition, the hydrophobic character of Mad was appreciated by the observation of aggregates at 1 mM Mad in hydro-alcoholic solution at pH 2 (see Supplemental Figure S8). Although the Φ_F of Mad is higher than that of Emo, its lower solubility results in a lower fluorescence signal, which reduces the quality of spectra recorded at λ_{488} or λ_{405} for Mad in solution. To note, this solubility problem was also observed in the cell culture medium after treatments, leading to the formation of aggregates still present after 18 h.

In vivo, very low fluorescence was detected in control (Ctr) and Lap-treated cells (Figure 4F, see Supplemental Figure S9 and Figure S10F). We define these signals as the autofluorescence threshold in tobacco BY-2 cells. For all other compounds, the emergence of fluorescence was clearly observed in treated BY-2 cells (5 min) being stable after 18 h treatments with either 25 µM (Figure 4A to 4E) or 50 µM (see Supplemental Figure S10A to S10E). Overall, excitation at λ_{405} resulted in a stronger fluorescence signal than at λ_{488}, but the opposite effect was observed with Qui- (Figure 4B) and Mad-treated cells (Figure 4D). As evidenced by our spectral analysis, only Fra-treated cells did not display fluorescence at a λ_{488} excitation (Figure 4E). Except for VH, all spectra recorded at 5 min after treatment are very similar (same λ_{Em} and shape) and independent of λ_{Ex} (Figure 4B-4E, see Supplemental Figure S10). PCA of the normalized average spectra

support the idea that the emission spectrum observed at λ_{488} in VH-treated cells shares similarities with those measured with Qui and especially Mad, but not with spectra found in Emo-treated cells (Figure 5B, see Supplemental Figure S11B to Figure S13B). Besides, the emission maxima observed in VH and Mad-treated cells (mostly in vesicular bodies) following excitation at λ_{488}, were centered at 539 nm and 575 nm. Even though the emission spectra recorded for VH- and Mad-cells share similarities with that of Qui-treated cells, the maximum of emission for Qui-treated cells was centered at 575 nm. These results strongly suggest that within the first minutes, VH and Mad lead to similar anthraquinones differing from those produced in both Emo- and Qui-treated cells. Interestingly, the fluorescence emission detected was usually observed first in the cytoplasm (see Supplemental Figure S14), and after 5 min in additional structures such as Golgi bodies (see Supplemental Figure S15), lipid droplets (see Supplemental Figure S16) and the ER (see Supplemental Figure S17). Specifically for Fra-treated cells excited at λ_{405}, a fluorescence emission was observed in the nucleus. Therefore, molecules are well absorbed by BY-2 cells and diffuse in different cell compartments following their polarity. The difference of shape and intensity between spectra collected in VH-treated cells suggests that at λ_{405} the monodeprotonated or complexed VH is detected in the cytoplasm and the ER, while at λ_{488} anthraquinones are predominantly observed in vesicular bodies such as lipid droplets and some Golgi bodies.

After 18 h, at λ_{488} or λ_{405} slight variations were detected in fluorescence intensities. In particular for anthranoids, it was found that their localization and emission spectra did not change significantly over time. Nevertheless, at λ_{405}, the shape of the emission spectrum in Mad-treated cells was found to be closely related to that of VH (Figure 4A and 4D). Also, other treatments have been associated either to the appearance of a new fluorescence emission signal in the primary vacuole (Figure 4A to 4C, see Supplemental Figure S10A to S10C), or to the translocation of an identical fluorescence signal from the nucleus into the primary vacuole as seen in Fra-treated cells (Figure 4E, see Supplemental Figure S10E). These results were further validated by a PCA analysis of the

normalized average spectra (Figure 5C and 5D, see Supplemental Figure S11C, S11D and Figure S13C, 13D), giving rise to clustering of fluorescence spectra according to putative structural similarities between the tested molecules in BY-2 cells. For instance, at λ_{488} (Figure 5D), the normalized average spectra of anthranoids-treated cells clustered, indicating that anthraquinones fluorescence was observed in contrast to Ctr, Lap and Fra, which do not fluoresce under these conditions. In addition, normalized average spectra collected at λ_{405} (Figure 5C) and at λ_{488} (Figure 5D) within the cytoplasm, ER and vesicular bodies in VH and Mad-treated cells were found to be similar and even closer after 18 h (Figure 5C and D) than after 5 min (Figure 5A and B). Therefore, they clustered in the PCA analysis. Conversely, the Emo normalized average spectra are significantly different at λ_{405} (Figure 5C) and slightly less different at λ_{488} (Figure 5D).

Taken together, these results strongly support that VH was transformed *in vivo* into anthraquinones with a structure closer to that of Mad than to that of Emo. In addition, PCA of standardized average spectra with excitation at 405 nm (λ_{405}) clearly confirmed the appearance of a new signal observed in the primary vacuole after 18 h treatment with VH-, Emo- and Qui-treated cells (Figure 5C), whereas it was not observed using excitation at 488 nm (λ_{488}). The fluorescence detected in the primary vacuole is similar to that detected in the cytoplasm for Emo and Qui unlike VH, for which the fluorescence observed in the primary vacuole is significantly different from that measured in the cytoplasm, ER and vesicular bodies. As a partial conclusion, SImaging analyses allowed us to accurately track the fluorescence of VH, related anthranoids and the coumarin (*i.e.,* fraxetin Fra) compared to Lap which exhibits no particular fluorescence in living cells. Moreover, the new fluorescence spectra observed after 5 min and 18 h supports the hypothesis that VH is metabolized into Mad anthraquinone-types *in vivo*. Interestingly, we detected signals at λ_{405} located in cell compartments whose acidity is below pK_{a1} values in Fra- and VH-treated cells (*i.e.,* pK_{a1} = 8.5 for Fra and pK_{a1} = 7.2 for VH). According to fluorescence of Fra and VH in model solution (Table 1), only complexes and especially LBSA species emit strong fluorescence at neutral pH. Thus, the bright signal observed at λ_{405} after feeding

with VH and Fra strongly support that part of Fra and VH are complexed *in cellula* and/or metabolized into related fluorescent compounds.

Fra and methyl-Fra derivatives prevail to Fra-glycosylated forms.

An increase in the polarity of given compounds typically results from their oxidation by oxygenases or glycosylation by glycosyltransferases. This metabolization enables then the sequestration of phenolic compounds into the primary cellular vacuole as described with Fra (Lefèvre et al., 2018; Stringlis et al., 2019). To identify metabolites of Fra, Qui, Emo, Mad and VH characterized by the fluorescence spectra detected by SImaging, non-targeted metabolomics of methanolic extracts from treated and non-treated BY-2 cells was carried out using UPLC-HRMS/MS. The results were compared to a database including the reference compounds and related metabolites deduced from *in silico* biotransformation. In this regard, 54 metabolites absent in the control extracts were annotated according to *m/z* of the parent ion and isotopic profile as compared to references or putative catabolites. In addition, hypothetical isomers and/or conjugates were annotated according to MS/MS fragments. As it cannot be excluded that after separation a loss of conjugates occurred in the MS source, the metabolites with different retention times (R_t) but similar *m/z* and MS/MS fragments were annotated as derivatives represented by putative isomers and/or conjugates.

All references except Lap (see Supplemental Figure S18D and Table S2) have been identified in corresponding methanolic extracts of BY-2 cells treated for 15 min or 18 h (Figure 6, see Supplemental Figure S18A to S18C and Table S3 to Table S5). The coumarin mixture annotated in the methanolic extracts from Fra-treated cells (Figure 6A) consists of 12 tri-oxygenated forms distributed in Fra and its supposed isomers (F1-F3), six methylated (F4-F9) and three glycosylated forms (F14-F16). The remaining metabolites correspond to tetra-oxygenated coumarins including reduced sideretin and two derivatives (F10-F12) together with another methoxylated form (F13). After 15 min, Fra quickly forms the more

polar F2 derivative. Simultaneously, both compounds may have been methylated (F8, F9) or glycosylated (F15, F16).

After 18 h, Fra, methylated forms F8 and F9 were significantly reduced in contrast to F2 derivative and F15 or F16 glycosylated forms, remaining constant (Figure 6A). In addition, the Fra derivative F1 abundance was increased 7-fold after 18 h, and other new methylated (F4, F5), hydroxylated (F10) as well as glycosylated (F14) forms were 6 to 33-fold more abundant (Figure 6A, see Supplemental Figure S18A). Thus, the annotated metabolites are consistent with those reported for BY-2 cells treated for 60 min with 20 µM of Fra (Lefèvre et al., 2018). Although the absolute quantitation was not performed, the Fra isomers or conjugates appeared to be a prevalent form for storage in the primary vacuole, while abundance of glycosylated derivatives did not significantly change over time. In comparison, Lefèvre et al. (Lefèvre et al., 2018) reported that 7 days-old BY-2 cells treated with Fra (20 µM) accumulate 63% of glycosylated derivatives. The metabolomics and SImaging results suggest that the spectral fingerprint observed at λ_{405} after 5 min and 18 h Fra treatments corresponds to a mixture of more polar Fra related metabolites rather than Fra itself. With this respect, Fra is metabolized and translocated from the cytoplasm and the nucleus to the primary vacuole for storage/sequestration in BY-2 cells (Figure 4E, Figure 6A and 6D). However, it was noticed that each group is mostly represented by a metabolite with an intermediate R_t (F2, F6, F11, F11) (Figure 6A, see Supplemental Table S3). Although BY-2 cells tend to produce other forms with lower R_t (more polar), it can be speculated that the later cannot be over accumulated due to putative cytotoxic effects. This is supported by the accumulation of methylated forms after 18 h, the latter being also reported to decrease negative effects of free hydroxyls from 1-hydroxycantin-6-one in *Ailanthus altissima* (Osoba and Roberts, 1994).

Metabolization of VH into anthrones and anthraquinones.

The metabolomic analyses of extracts isolated from anthranoids treated cells after 15 min and 18 h highlighted specificities. For instance, Qui (Q6) and five of

its derivatives (Q1-Q5) were found exclusively in Qui-treated cells extracts (Figure 6B, see Supplemental Table S4) while Emo-, Mad- and VH-treated cells shared a few common metabolites (Figure 6C, see Supplemental Table S5). We noted an absence of methylated, hydroxylated or glycosylated forms, which may be explained by the unusual 4-OH group of Qui found in traces as reported in *Cassia obtusifolia* extracts (Rossi et al., 2010). In contrast, most natural anthranoids are found to be hydroxylated at all other positions except the position 2 associated to carboxylic acid progenitors (Gill, 2001). Accordingly, it can be speculated that Q1-Q5 are five isomers resulting either from a chemical tautomerization/isomerization or from redox processes (Fain et al., 2006; Batchelor-McAuley et al., 2011). Meanwhile, it cannot be excluded that 1-OH was removed and the position C5 or C7 hydroxylated as reported for Emo (Gill, 2001; Chiang et al., 2010). The specific detection of Qui in related methanolic cell extracts is consistent with its fluorescence detected by SImaging at λ_{488}. However, the non-targeted metabolomics pointed out that the Qui fluorescence detected in the cytoplasm, lipid droplets and some Golgi bodies may be related to Q1-Q5 derivatives too. In the absence of Q1-Q5 references, we were not able to confirm whether these derivatives or Qui contributed to the fluorescence observed and especially that in the primary vacuole (λ_{405}). Thus, it can also be assumed that the latter would be originated from other non-annotated metabolites.

In VH-, Mad-, Emo-treated cells, the Emo (A8) and eight of its derivatives (A1-A7, A9) have been detected (Figure 6C, see Supplemental Table S5). In addition, five methylated (A10-A14), two hydroxylated (A15, A16), two methoxylated (A17, A18) and four glycosylated (A24-A27) Emo derivatives were significantly detected only in Emo-treated cells. Surprisingly, Emo and its A1-A6 derivatives were almost exclusive of Emo-treated cells and after 18 h the A1-A5 abundance significantly increased. In contrast, the Emo derivatives A7 and A9 were specific to Mad and VH-treated cells. This agrees with SImaging and PCA results obtained for Emo-treated cells at 5 min and 18 h. Indeed, the fluorescence observed mostly in the cytoplasm at λ_{405} and λ_{488} corresponds to a specific

spectral fingerprint of Emo and more likely to A6 content that is unchanged in our metabolomic data at both 15 min and 18 h. In contrast, it can be proposed that the fluorescence observed in the primary vacuole at λ_{405} after 18 h, is from a mixture of the most hydrophilic derivatives (A1-A5), glycosylated (A24, A25) or hydroxylated (A15, A16) forms, being significantly increased after 18 h as compared to 15 min (Figure 6C and 6D). Other metabolites such as VH (A23) as well as Mad anthrone and two putative isomers (A19-A21) were only detected in VH-treated cells, while Mad (A22) was found in VH and Mad-treated cells.

DISCUSSION

For years, the metabolism, biosynthesis and bioactivity of anthranoids were studied through chemical analysis of metabolites after feeding experiments with radiolabeled precursors (Gill, 2001), genome mining (Chiang et al., 2010; Kang et al., 2020) and bioassays (François et al., 1999; Gallé, 2015), respectively. Our study demonstrates that SImaging is an additional sensitive and suitable tool for the observation of anthranoids *in vivo*. In depth, unlike classical microscopy, SImaging allowed us to localize and discriminate VH and related fluorescent metabolites over time, in living cells. Still, UV-Vis spectrophotometric and spectrofluorometric analyses were crucial not only to characterize unbiasedly the fluorescence of compounds in solution, but also to evidence the influence of pH or complex formation with cations and protein on it. In fact, SImaging was already used to study the role of coumarins such as scopoline, fraxin and esculin in the iron metabolism of *A. thaliana* roots (Robe et al., 2021), but not fraxetin Fra (the fraxin genuine). Even though Fra is reported as a non-fluorescent coumarin (Tsai et al., 2018; Lefèvre et al., 2018), our study evidenced that under alkaline or complexation conditions, its fluorescence is enhanced and modulated depending on the ligand (Table 1). Surprisingly, the Fra fluorescence spectra recorded by SImaging and spectrofluorimetry were significantly different except for Fra-BSA complex (Table 1, Figure 2F, see Supplemental Figure S3B and SD). In this context, the overlapping of fluorescence spectra from free and complexed coumarins is limiting for a clearcut discrimination by SImaging. In fact, extracting

spectra to unmix fluorescence signals was reported (Robe et al., 2021), however our data indicate a cellular colocalization of molecular species that are therefore barely distinguishable even with acquisition settings of the fluorescent signal at 9 nm/channel. By contrast, the anthranoids fluorescence spectra are consistent between SImaging and spectrofluorimetry analyses, allowing good identification of fluorescent species observed. The fruitful combination of SImaging with the non-targeted metabolomics was particularly effective in identifying at 5 min and after 18h, not only key anthranoids metabolites such as madagascine anthrone, Mad and putative emodin derivatives, but also a battery of Fra methylated, hydroxylated and glycosylated derivatives. To note, except sideretin, the Fra methylated and hydroxylated derivatives annotated in our study were not taken into account in the study of coumarin/iron metabolism in *A. thaliana* (Tsai et al., 2018; Robe et al., 2021). As coumarin accumulation and trafficking is a complex and dynamic process, these derivatives also previously reported in *N. tabacum* (Lefèvre et al., 2018), might be considered for further study in *A. thaliana* as well. Therefore, non-targeted metabolomics is a clear advantage in elucidating unraveled metabolic pathways, identifying unintended and scavenged metabolites prior to targeted metabolomics, being more adapted for systematic quantitation of known metabolites.

For the first time, our study provides an overview of both metabolization processes and subcellular compartments implied in anthranoids metabolism in plants, involving at least five cell compartments after VH treatments (primary vacuole, cytoplasm, ER, Golgi bodies and lipid droplets vesicular bodies). The cell compartments labelled by anthranoids are consistent with the ER, the cytosol and the primary vacuole suggested by Han et al. in Rubiaceae (Han et al., 2001), and the phenotype observed in melanoma cell culture treated with 10 µM Emo or Qui (Verebova et al., 2016). Collocation experiments with plastids marker was not performed, but in addition to Golgi bodies and lipid droplets, a part of spherical structures labelled by anthranoids could corresponds to plastids as reported in *Morinda citrifiolia* (Yamamoto et al., 1987). Outstandingly, the acetyl vismione D (C3-O-geranyl) was assumed to be not fluorescent enough for

observation with fluorescence microscopy (Gallé, 2015), here, we have characterized the fluorescence *in cellula* of VH as well as its degradation products known as madagascine anthrone and anthraquinone. VH is not only converted to Mad anthrone and Mad under oxidative conditions such as in DMSO indeed, but *in vivo* too. Interestingly, the anthrone A20 remains well detected, whereas in DMSO Mad and bianthrone prevail after 8 h (Gallé, 2015). After 18 h the amount of VH, Mad and A20 remained insignificantly altered in VH-treated cells, while the Mad anthrone derivatives A19, A21 were not detected anymore and Mad abundance considerably decreased in Mad-treated cells after 18 h. Unexpectedly, Mad, which is the less polar molecule (R_t = 11.73 min) was metabolized into A9 derivative rather than Emo (A8), suggesting that in BY-2 cells other reactions occur with Mad prior to loss of the prenyl moiety. With this respect, the bright fluorescence in VH-treated cells observed by SImaging at λ_{405} mainly in the cytoplasm (see Supplemental Figure S14C), Golgi bodies (see Supplemental Figure S15) and the ER (see Supplemental Figure S17) corresponds to a mixture of anthranol forms of Mad anthrone and VH and/or complexes, the anthrones being weakly fluorescent (Fujii et al., 1997). It can be proposed that pH, intracellular O_2, redox levels or chelation with cations or proteins may stabilize these forms (Hlasiwetz and Grabowski, 1867; Cameron et al., 1976; Fujii et al., 1997), detected by SImaging in the different subcellular compartment. However, we could not discriminate if the fluorescence observed at λ_{405} in the primary vacuole of VH-treated cells after 18 h corresponds to a non-annotated metabolite or to VH-LH_2 and/or Mad anthrone neutral forms. Since the metabolomic analysis evidenced similar anthraquinones between Mad and VH-treated cells extracts, the spectral fingerprint observed by SImaging at λ_{488} corresponds to Mad and likely the specific Emo A9 and/or A7 derivatives.

Taken together, these results point out that C3-OH substitution of anthranoids is a key position influencing both the anthranoids fluorescence and metabolization in BY-2 cells depending on its nature. A free 3-OH allows anthranoids metabolization into very polar Emo derivatives (A1-A6) as well as hydroxylated, methylated or glycosylated forms dedicated to a vacuolar storage. In contrast

when this position is substituted with a prenyl group as for VH or Mad, the metabolization is markedly altered producing hydrophobic Emo derivatives (A7 and A9). As we were not able to decipher whether enzymatic or chemical reactions contributed to putative oxidation and/or isomerization processes, we can only pinpoint that C3-O-prenylated anthranoids metabolization calls for targeting to lipid droplets, Golgi bodies and to the ER subcellular location. On a recurring basis, because VH and Mad anthrone were automatically detected in VH reference solution, it can be speculated that both chemical isomerization/ tautomerization and VH deacetylation occur *in vivo* too. However, the remarkable distribution of methylated, hydroxylated, glycosylated and other derivatives in most treatments is consistent with a well-orchestrated subset of enzymes as it has been described for Fra or Emo (Gill, 2001; Tsai et al., 2018). To clarify these aspects, in the future it would be interesting to purify fluorescent labelled organellar fractions and analyze the transcriptome and proteome. From a general point of view, the total contents of metabolites detected in Emo and Qui-treated cells were doubled after 18 h, halved for Mad- or VH-treated cells and remains constant in Fra-treated cells (Figure 6D). Although, related metabolites seem to be accumulated over time in Emo, Qui and Fra-treated cells, the abundance of references was 26, 3.5 and 16 times lower after 18 h, confirming their metabolization/storage. In contrast, the Mad and VH abundance in treated cells changed weakly, supporting the fact that both VH and Mad are transformed *in vivo* into non-annotated metabolites and metabolization rate of prenylated anthranoids in BY-2 cells is limited.

Interestingly, our data unambiguously evidenced that tobacco BY-2 cells are competent to take up and metabolize anthranoids, not produced by *N. tabacum* plants. Due to its low cost, low autofluorescence and heterogeneous metabolism, the BY-2 cell model is of particular interest and could undoubtedly serve to study metabolism and localization of other molecules of interest in living organisms. As long as anthranoids and other naturally occurring fluorescent compounds are valuable, it would be interesting to extend this study to investigate unknown aspects of the biosynthesis pathways and the influence of biotic and abiotic

552 factors on the metabolism of anthranoids and other fluorescent compounds.
553 From another point of view, the developed approach offers interesting
554 perspectives in the medical field, as VH and similar compounds have been
555 described for their antimalarial properties (François et al., 1999; Mazimba et al.,
556 2013; Gallé, 2015), but the biological targets as well as mechanisms of action
557 remain unknown. Last, it would be interesting to reproduce experiments in red
558 blood cells infected by *P. falciparum* treated with VH and analogs, therefore
559 opening an avenue to fluorescence localization/structure/activity relationships
560 studies. To be deciphered, the complexity of metabolic pathways requires more
561 than ever multifactorial analyses of living organisms, this SImaging approach
562 coupled with non-targeted metabolomics allows efficient characterization of
563 subcellular location and bioconversion of fluorescent metabolites in living plant
564 cells.

565
566 **METHODS**

567 **Chemicals**

568 Fraxetin (7,8-dihydroxy-6-methoxy-coumarin), quinizarin (1,4-dihydroxy-
569 anthraquinone), emodin (1,3,8-trihydroxy-6-methyl-9,10-anthracenedione),
570 lapachol (2-hydroxy-3-(3-methyl-2-butenyl)-1,4-naphthoquinone) were purchased
571 from Sigma-Aldrich. Vismione H and madagascine were obtained from PGE2
572 fraction of *Psorospermum glaberimum* as previously described (Gallé, 2015).
573 Other chemicals were from usual commercial sources with the highest purity
574 available.

575

576 **Spectrofluorimetric analyses**

577 First, the pK_a values of the selected compounds were measured in EtOH/water
578 (see supplemental Table S1). Then, Different solutions of the pure compounds at
579 0.01 mg/ml were prepared from stock solutions in EtOH at 1 mg/mL and then
580 diluted either in EtOH/H_2O 1:1 *v/v*, 0.1 M NaCl adjusted with HCl 10^{-2} M (pH 2),
581 $Na_2B_4O_7$ 0.01 M or NH_4HCO_3 (pH 10), NaOH 10^{-2} M (pH 12) or in EtOAc. The
582 absorbance spectra of (de)protonated species in solution were measured from

260 – 800 nm using a Cary 5000 UV-Vis.-NIR spectrophotometer (Agilent, Santa Clara USA) prior to any fluorescence analysis. Fluorescence spectra of solutions diluted 10-fold were recorded with 3.5 mL Suprasil® quartz optical cells of 10 mm pathlength using a LS-50B spectrofluorimeter monitored with UVWinlab 5.1 software (Perkin Elmer, Waltham USA). For each compound, fluorescence emission spectrum was recorded by exciting close or at the maximum absorption wavelength, and instrumental parameters were adjusted to a scanning speed of 400 nm/min and excitation/emission bandwidths adjusted between 4.5 and 15 nm depending on the conditions. The fluorescence spectra of each compound were established by successive determination of the excitation (λ_{Ex}) and emission (λ_{Em}) maxima. A FluoroMax-4 spectrofluorimeter (HORIBA, Kyoto Japan) was then used to accurately determine the quantum yields of anthranoids at 0.001 mg/ml with one exception (0.0015 mg/mL for emodin) in solutions at pH 2 and at pH 10 only for VH and Fra. The quantum yields of the fluorescent species (Φ_F) were calculated by using the equation below with either rhodamine 6G (R6G) or cresyl violet references.

$$\Phi_F = \Phi_R \frac{\int I_F A_R n_F^2}{\int I_R A_S n_R^2}$$

Φ_R corresponds to the quantum yield of reference. The indices F and R denote sample and reference, respectively. The integrals over I represent areas of the corrected emission spectra, A is the optical density at the excitation wavelength and n_R and n_S correspond to the refractive index of the reference and the sample solutions, respectively.

Ca^{2+} and Mg^{2+} chelating assay

Fresh stock solution of VH (2.6 mM) in EtOH was further diluted 100-fold in EtOH/H_2O 1:1 *v/v* containing 0.1 M NaCl. UV-Vis spectrophotometric titrations of the solutions were then carried out by adding increasing amounts of $CaCl_2$ or $MgCl_2$ and monitored using a Cary 5000 UV-Vis-NIR (Agilent, Santa Clara USA). 0.1 M $CaCl_2$ or $MgCl_2$ (25 µL) prepared in water were successively added to 2 mL of the ligand solution (VH: 26 µM). The Ca^{2+} and Mg^{2+} chelating properties of

VH were also investigated by fluorescence emission, adding 0.1 M $CaCl_2$ (150 and 300 µL) or 0.1 M $MgCl_2$ solutions to a 2.6 µM VH solution. The quantum yields of the Ca^{2+} and Mg^{2+} chelates with VH were measured as described in the *spectrofluorimetric analysis* section.

Plant material and treatment

The *Nicotiana tabacum* cv. Bright Yellow 2 (tobacco BY-2) cell suspension was made available by Toshiyuki Nagata (Tokyo University, Japan) and cultivated at 26 °C, on a rotary shaker set at 140 rpm in the dark, in modified Murashige and Skoog (MS) medium as reported (Hemmerlin and Bach, 2000). For treatments, 7-days old cells were diluted five-fold into fresh MS medium and distributed (3 mL) in 6-well culture plates (Sarstedt, Nümbrecht Germany) containing 25 or 50 µM of phenolic compounds. SImaging acquisitions were carried out either after 5 min incubation or after 18 h.

Spectral imaging (SImaging) microscopy

Treated cells or pure compounds at 1 mM in the solutions at pH 2, pH 10 and pH 12 were observed using a LSM780 confocal laser microscope (Carl Zeiss, Jena Germany) equipped with an inverted Zeiss AxioObserver Z1, a Plan-Apochromat 20x/0.8 M27 objective, a numerical zoom adjusted to 2.8 with a laser strength of 5 %. Images and emission spectra were acquired using the excitation wavelengths at 405 (λ_{405}) and 488 nm (λ_{488}) with the emission light collected into multiple channels incremented by 9 nm from 415 to 664 nm and 498 to 664 nm, respectively. The lambda view images correspond to superimposed fluorescence recorded in each channel according to natural light spectrum. The spectral analysis was done after the extraction of emission spectra from images by manual component extraction of 1 µm circles in different cell compartment labelled by a fluorescence. Images were exported from Zen v2 software (Zeiss, Jena Germany) and assembled in figure using ImageJ v1.53d.

Spectral data analysis

The dataset consisted of 10 spectra/cell collected from five cells in three independent biological replicates for each treatment, at 25 and 50 µM, after 5 min and 18 h. Intensities per channels of each spectrum were averaged per cell and normalized to 1 before statistical analysis with R software V4.0.0 (GNU GPLv2, R Core Team) and RStudio V 1.2.5001 (AGPLv3, RStudio) using the ChemoSpec package V5.2.12. A distant matrix was established for each dataset applying the Pearson's correlation coefficient, and a robust principal component analysis (PCA) was performed. The same procedure was used with solutions of pure compounds to analyze 10 spectra/acquisition in triplicate.

Non-targeted metabolomic analysis

Freeze-dried BY-2 cells (25 mg) treated for 15 min or 18 h with 50 µM of each compound were extracted in MeOH (3x300 µL), sonicated during 20 min at 80 kHz (Fisherbrand^{TM} S-series), then the total extract was filtered prior to analysis. Standard solution at 0.002 mg/mL in EtOH and MeOH extracts from three independent biological replicates were analyzed by non-targeted metabolomics approach performed on the UltiMate 3000 UHPLC system (Thermo) coupled to the ImpactII (Bruker) high resolution Quadrupole Time-of-Flight (QTOF) as previously described (Villette et al., 2018). Samples were kept at 4°C, 3 µL were injected with a washing step after sample injection with a wash solution (H_2O/MeOH, 90/10, v/v, 150 µL). The spectrometer was equipped with an electrospray ionization (ESI) source and operated in positive ion mode on a mass range from 20 to 1000 Da with a spectra rate of 2Hz in AutoMS/MS fragmentation mode. The end plate offset was set at 500 V, capillary voltage at 2500 V, nebulizer at 2 Bar, dry gas at 8 $L.min^{-1}$ and dry temperature at 200°C. The transfer time was set at 20-70µs and MS/MS collision energy at 80-120% with a timing of 50-50% for both parameters. The MS/MS cycle time was set to 3 seconds, absolute threshold to 816 cts and active exclusion was used with an exclusion threshold at 3 spectra, release after 1 min and precursor ion was reconsidered if the ratio current intensity/previous intensity was higher than 5. Raw data were processed in MetaboScape 4.0 software (Bruker): molecular

features were considered and grouped into buckets containing one or several adducts and isotopes from the detected ions with their retention time and MS/MS information when available. The parameters used for bucketing are a minimum intensity threshold of 1000, a minimum peak length of 3 spectra, a signal-to-noise ratio (S/N) of 3 and a correlation coefficient threshold set at 0.8. The $[M+H]^+$, $[M+Na]^+$, $[M+K]^+$ and $[M+NH4]^+$ ions were authorized as possible primary ions. The obtained list of buckets was annotated using a custom analyte list derived from *in silico* predicted metabolites (catabolites and conjugates) of the compounds of interest. The *in silico* prediction was performed using MetabolitePredict 2.0 (Bruker) as previously described (Villette et al., 2019). Briefly, 79 biotransformation rules were used to predict metabolites over 2 generations. The maximum allowed variation on the mass (*m/z*) was set to 3 ppm, and the maximum mSigma value (assessing the good fitting of isotopic patterns) was set to 30. The changes in abundance of each metabolites annotated were appreciated using a statistical analysis by comparing the area obtained under the chromatogram curve of the different metabolites analyzed in triplicates. The homogeneity of the variance was checked with a Levene prior to a Kruskal-Wallis test, followed by multi comparison procedure using post-hoc Dunnett's test.

SUPPLEMENTAL DATA

Supplemental Figure S1. Influence of pH on absorption properties of studied phenolic compounds

Supplemental Figure S2. Fluorescence emission/excitation spectra of studied compounds in solution at different pH

Supplemental Figure S3. Normalized fluorescence excitation/emission and absorption spectra of $LNH4^+$ and LBSA complexes

Supplemental Figure S4. UV-Vis. absorption titration of vismione H by Ca(II)

Supplemental Figure S5. UV-Vis. absorption titration of vismione H by Mg(II).

Supplemental Figure S6. Absorption and fluorescence emission spectra of anthranoids and fraxetin LBSA complexes

Supplemental Figure S7. Corrected Absorption and fluorescence properties of fraxetin and vismione LBSA complexes.

Supplemental Figure S8. Images of fluorescent species from studied phenolic compounds in solution observed by SImaging.

Supplemental Figure S9. Normalized average spectra and images from SImaging analysis of lapachol treated cells.

Supplemental Figure S10. Fluorescence spectra and images of BY-2 cells treated by 50µM of phenolic compounds prior to observation using SImaging

Supplemental Figure S11. Distant matrix of normalized average spectra obtained by SImaging analysis of By-2 cells were treated or not with 25 µM of phenolic compounds.

Supplemental Figure S12. PCA of normalized average spectra obtained by SImaging analysis of cells treated or not with 50 µM of phenolic compounds

Supplemental Figure S13. Distant matrix of normalized average spectra obtained by SImaging analysis of cells treated or not with 50 µM of phenolic compounds

Supplemental Figure S14. Anthranoids fluorescence locates in the cytoplasm of living BY-2 cells labeled with fluorescein diacetate viability marker after 18 h of treatment.

Supplemental Figure S15. Vismione H and related anthraquinones fluorescence locate in the Golgi body of BY-2 cells.

Supplemental Figure S16. Vismione H related anthraquinones fluorescence locate in lipid droplets of living BY-2 cells

Supplemental Figure S17. Anthranoids fluorescence locate in the endoplasmic reticulum of BY-2 cells.

Supplemental Figure S18. Non-targeted metabolomics of BY-2 cells treated by studied phenolic compounds

Supplemental Table S1. pKa values of pure compounds measured in solution.

Supplemental Table S2. Metabolites identified in non-targeted metabolomic analysis of MeOH extracts from BY-2 cells treated with 50 µM Lap

Supplemental Table S3. Metabolites identified in non-targeted metabolomic analysis of MeOH extracts from BY-2 cells treated with 50 µM Fra

Supplemental Table S4. Metabolites identified in non-targeted metabolomic analysis of MeOH extracts from BY-2 cells treated with 50 µM Qui.

Supplemental Table S5. Metabolites and fragments identified in non-targeted metabolomic analysis of MeOH extracts from BY-2 cells treated with 50 µM Emo, Mad and VH.

ACKNOWLEDGMENTS

This work was supported by the French National Centre for Scientific Research and the University of Strasbourg. We thank Dr. Gilles Ulrich (Institut de Chimie des Procédés pour l'Énergie, l'Environnement et la Santé, Strasbourg) for access to the spectrofluorometer to establish reference spectra and quantum yields. We thank to Pr. Thomas J. Bach (Institut de Biologie Moléculaire des Plantes, Strasbourg) for sharing collection of phenolic compounds and to Dr. Dimitri Heintz for access to mass spectrometry equipments (metabolomics facility, IBMP). We are also grateful to Stephanie Riché and Dr. Sridevi Ramanoudjame (Laboratoire d'Innovation Thérapeutique, Strasbourg) for excellent technical assistance to purify vismione H. We acknowledge helpful criticism and discussion with Dr. Romain Duval and Dr. Elisabeth Davioud-Charvet.

AUTHOR CONTRIBUTIONS

Q.C., C.V.-S., A.H., M.E., J.M., N.G., designed the research; Q.C., V.M., M.E., performed research; Q.C., J.-B.G., N.W., M.E., V.M., C.V., J.M., contributed new reagents/analytic tools; Q.C., V.M., C.V., M.M.E., analyzed data; and Q.C., J.-B.G., V.M., C.V., M.M.E., M.E., H.S., A.H., C.V.-S., wrote the article.

REFERENCES

Batchelor-McAuley, C., Dimov, I.B., Aldous, L., and Compton, R.G. (2011).

The electrochemistry of quinizarin revealed through its mediated reduction of oxygen. Proc. Natl. Acad. Sci. **108**: 19891–19895.

Binzel, M.L., Hess, F.D., Bressan, R.A., and Hasegawa, P.M. (1988). Intracellular Compartmentation of Ions in Salt Adapted Tobacco Cells. Plant Physiol. **86**: 607–614.

Cameron, D., Edmonds, J., and Raverty, W. (1976). Oxidation of emodin anthrone and stereochemistry of emodin bianthrone. Aust. J. Chem. **29**: 1535.

Carden, D.E., Walker, D.J., Flowers, T.J., and Miller, A.J. (2003). Single-Cell Measurements of the Contributions of Cytosolic Na^+ and K^+ to Salt Tolerance. Plant Physiol. **131**: 676–683.

Chiang, Y.-M., Szewczyk, E., Davidson, A.D., Entwistle, R., Keller, N.P., Wang, C.C.C., and Oakley, B.R. (2010). Characterization of the Aspergillus nidulans Monodictyphenone Gene Cluster. Appl. Environ. Microbiol. **76**: 2067–2074.

Conéjéro, G., Noirot, M., Talamond, P., and Verdeil, J.-L. (2014). Spectral analysis combined with advanced linear unmixing allows for histolocalization of phenolics in leaves of coffee trees. Front. Plant Sci. **5**.

Dong, X., Fu, J., Yin, X., Cao, S., Li, X., Lin, L., Huyiligeqi, and Ni, J. (2016). Emodin: A Review of its Pharmacology, Toxicity and Pharmacokinetics: Emodin: Pharmacology, Toxicity and Pharmacokinetics. Phytother. Res. **30**: 1207–1218.

Dudev, T. and Lim, C. (2004). Monodentate versus Bidentate Carboxylate Binding in Magnesium and Calcium Proteins: What Are the Basic Principles? J. Phys. Chem. B **108**: 4546–4557.

Duval, R., Cottet, K., Blaud, M., Merckx, A., Houzé, S., Grellier, P., Lallemand, M.-C., and Michel, S. (2020). A Photoalkylative Fluorogenic Probe of Guttiferone A for Live Cell Imaging and Proteome Labeling in Plasmodium falciparum. Molecules **25**: 5139.

Duval, R. and Duplais, C. (2017). Fluorescent natural products as probes and tracers in biology. Nat. Prod. Rep. **34**: 161–193.

Elkazaz, S. and Jones, P.B. (2010). Photochemical Hydroxylation of 1-Methyl-9,10-anthraquinones: Synthesis of 9′-Hydroxyaloesaponarin II. J. Org. Chem. **75**: 412–416.

Fain, V.Ya., Zaitsev, B.E., and Ryabov, M.A. (2006). Tautomerism of anthraquinones: V. 1,5-Dihydroxy-9,10-anthraquinone and its substituted derivatives. Russ. J. Org. Chem. **42**: 1662–1667.

François, G., Steenackers, T., Assi, L.A., Steglich, W., Lamottke, K., Holenz, J., and Bringmann, G. (1999). Vismione H and structurally related anthranoid compounds of natural and synthetic origin as promising drugs against the human malaria parasite Plasmodium falciparum : structure-activity relationships. Parasitol. Res. **85**: 582–588.

Friedman, M. and Jürgens, H.S. (2000). Effect of pH on the Stability of Plant Phenolic Compounds. J. Agric. Food Chem. **48**: 2101–2110.

Fujii, T., Mishima, S., Tanaka, N., Kawauchi, O., Kodaira, K., Nishikiori, H., and Kawai, Y. (1997). Absorption and fluorescence spectra of 9-anthrol and its chemical species in solution. Res. Chem. Intermed. **23**: 829–839.

Furumoto, T. and Jindai, A. (2008). Isolation and Photoisomerization of a New

Anthraquinone from Hairy Root Cultures of *Sesamum indicum*. Biosci. Biotechnol. Biochem. **72**: 2788–2790.

Gallé, J.-B. (2015). Pharmacochimie d'anthranoïdes issus du genre Psorospermum (Hypericaceae): isolement, activités antiparasitaires et synthèse d'analogues structuraux Jean-Baptiste Galle.

Gill, M. (2001). The Biosynthesis of Pigments in Basidiomycetes. Aust. J. Chem. **54**: 721.

Giusti, M.M. and Wrolstad, R.E. (2001). Characterization and Measurement of Anthocyanins by UV-Visible Spectroscopy. Curr. Protoc. Food Anal. Chem. **00**: F1.2.1-F1.2.13.

Guo, W., Chen, S., Hussain, N., Cong, Y., Liang, Z., and Chen, K. (2015). Magnesium stress signaling in plant: Just a beginning. Plant Signal. Behav. **10**: e992287.

Han, Y.-S., Van der Heijden, R., and Verpoorte, R. (2001). Biosynthesis of anthraquinones in cell cultures of the Rubiaceae. Plant Cell Tissue Organ Cult. **67**: 201–220.

Hemmerlin, A. and Bach, T.J. (2000). Farnesol-induced cell death and stimulation of 3-hydroxy-3-methylglutaryl-coenzyme A reductase activity in tobacco cv bright yellow-2 cells. Plant Physiol. **123**: 1257–1268.

Hepler, P.K. (2005). Calcium: A Central Regulator of Plant Growth and Development. Plant Cell **17**: 2142–2155.

Hlasiwetz, H. and Grabowski, A. (1867). Mittheilungen aus dem chemischen Laboratorium in Innsbruck. I. Ueber die Carminsäure; Ann. Chem. Pharm. **141**: 329–345.

Kang, S.-H. et al. (2020). Genome-enabled discovery of anthraquinone biosynthesis in Senna tora. Nat. Commun. **11**: 5875.

Lefèvre, F., Fourmeau, J., Pottier, M., Baijot, A., Cornet, T., Abadía, J., Álvarez-Fernández, A., and Boutry, M. (2018). The Nicotiana tabacum ABC transporter NtPDR3 secretes O-methylated coumarins in response to iron deficiency. J. Exp. Bot. **69**: 4419–4431.

Martinière, A., Bassil, E., Jublanc, E., Alcon, C., Reguera, M., Sentenac, H., Blumwald, E., and Paris, N. (2013). In Vivo Intracellular pH Measurements in Tobacco and *Arabidopsis* Reveal an Unexpected pH Gradient in the Endomembrane System. Plant Cell **25**: 4028–4043.

Mazimba, O., Nana, F., and Singh, G.S. (2013). Xanthones and Anthranoids from the Medicinal Plants of Africa. In Medicinal Plant Research in Africa, V. Kuete, ed (Elsevier), pp. 393–434.

Nagata, T., Nemoto, Y., and Hasezawa, S. (1992). Tobacco BY-2 Cell Line as the "HeLa" Cell in the Cell Biology of Higher Plants. In International Review of Cytology (Elsevier), pp. 1–30.

Osoba, O.A. and Roberts, M.F. (1994). Methyltransferase activity in Ailanthus altissima cell suspension cultures. Plant Cell Rep. **13**: 277–281.

Robe, K. et al. (2021). Coumarin accumulation and trafficking in *Arabidopsis thaliana* : a complex and dynamic process. New Phytol. **229**: 2062–2079.

Rossi, S., Tabolacci, C., Lentini, A., Provenzano, B., Carlomosti, F., Frezzotti, S., and Beninati, S. (2010). Anthraquinones danthron and quinizarin

exert antiproliferative and antimetastatic activity on murine B16-F10 melanoma cells. Anticancer Res. **30**: 445–449.

Sedaira, H., Idriss, K.A., Seleim, M.M., and Abdel-Aziz, M.S. (1998). Use of Quinizarin as a Spectrophotometric Reagent for MgO Content Analysis of Portland Cement and Cement Clinker. Monatshefte Für Chem. Chem. Mon. **129**: 49–58.

Shen, J., Zeng, Y., Zhuang, X., Sun, L., Yao, X., Pimpl, P., and Jiang, L. (2013). Organelle pH in the Arabidopsis Endomembrane System. Mol. Plant **6**: 1419–1437.

Srinivas, G., Babykutty, S., Sathiadevan, P.P., and Srinivas, P. (2007). Molecular mechanism of emodin action: Transition from laxative ingredient to an antitumor agent. Med. Res. Rev. **27**: 591–608.

Stringlis, I.A., de Jonge, R., and Pieterse, C.M.J. (2019). The Age of Coumarins in Plant–Microbe Interactions. Plant Cell Physiol. **60**: 1405–1419.

Talamond, P., Verdeil, J.-L., and Conéjéro, G. (2015). Secondary Metabolite Localization by Autofluorescence in Living Plant Cells. Molecules **20**: 5024–5037.

Tissier, A., Ziegler, J., and Vogt, T. (2014). Specialized Plant Metabolites: Diversity and Biosynthesis. In Ecological Biochemistry, G.-J. Krauss and D.H. Nies, eds (Wiley-VCH Verlag GmbH & Co. KGaA: Weinheim, Germany), pp. 14–37.

Tsai, H.-H., Rodríguez-Celma, J., Lan, P., Wu, Y.-C., Vélez-Bermúdez, I.C., and Schmidt, W. (2018). Scopoletin 8-Hydroxylase-Mediated Fraxetin Production Is Crucial for Iron Mobilization. Plant Physiol. **177**: 194–207.

Verebova, V., Belej, D., Joniova, J., Jurasekova, Z., Miskovsky, P., Kozar, T., Horvath, D., Stanicova, J., and Huntosova, V. (2016). Deeper insights into the drug defense of glioma cells against hydrophobic molecules. Int. J. Pharm. **503**: 56–67.

Villette, C., Maurer, L., Wanko, A., and Heintz, D. (2019). Xenobiotics metabolization in Salix alba leaves uncovered by mass spectrometry imaging. Metabolomics **15**: 122.

Villette, C., Zumsteg, J., Schaller, H., and Heintz, D. (2018). Non-targeted metabolic profiling of BW312 Hordeum vulgare semi dwarf mutant using UHPLC coupled to QTOF high resolution mass spectrometry. Sci. Rep. **8**.

Waters, B.M. (2011). Moving magnesium in plant cells: Commentary. New Phytol. **190**: 510–513.

Yamamoto, H., Tabata, M., and Leistner, E. (1987). Cytological changes associated with induction of anthraquinone synthesis in photoautotrophic cell suspension cultures of Morinda lucida. Plant Cell Rep. **6**: 187–190.

FIGURES AND TABLES

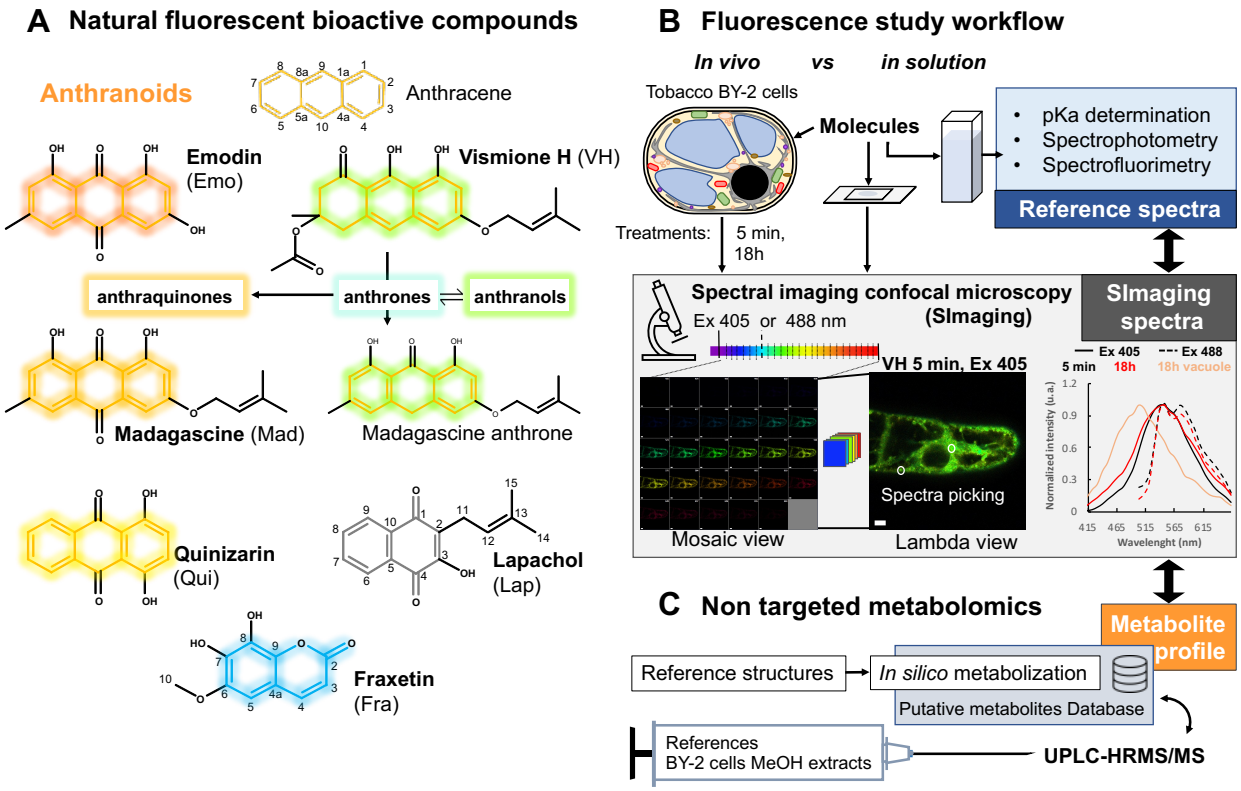

Figure 1. Overview of natural fluorescent bioactive anthranoids and the original approach used to study their localization and biotransformation in living cells. **(A)** Chemical structures of anthranoids characterized by the anthracene skeleton (orange skeleton) as compared to other phenolic compounds such as the naphtoquinone lapachol (Lap, black skeleton) and the coumarin fraxetin (Fra, blue skeleton). In dimethylsulfoxide (DMSO), vismione H (VH) degrades quickly into anthrones (weak turquoise fluorescence) being in equilibrium with anthranol tautomers (strong green yellowish) and oxidized into anthraquinones such as emodin (Emo), madagascine (Mad) or quinizarin (Qui) (yellow to red fluorescence). **(B-C)** Spectral imaging and non-targeted metabolomic workflow to characterize biotransformation of fluorescent anthranoids in tobacco BY-2 cells. **(B)** Fluorescence of selected anthranoids is evaluated in solution, then these anthranoids (25 or 50 µM) are used to feed cells for confocal spectral imaging microscopy at 5 min and 18 h after feeding. **(C)** Non-targeted metabolomics workflow implementing high-resolution mass spectrometry analysis of methanolic extracts from cells characterized in **(B)**.

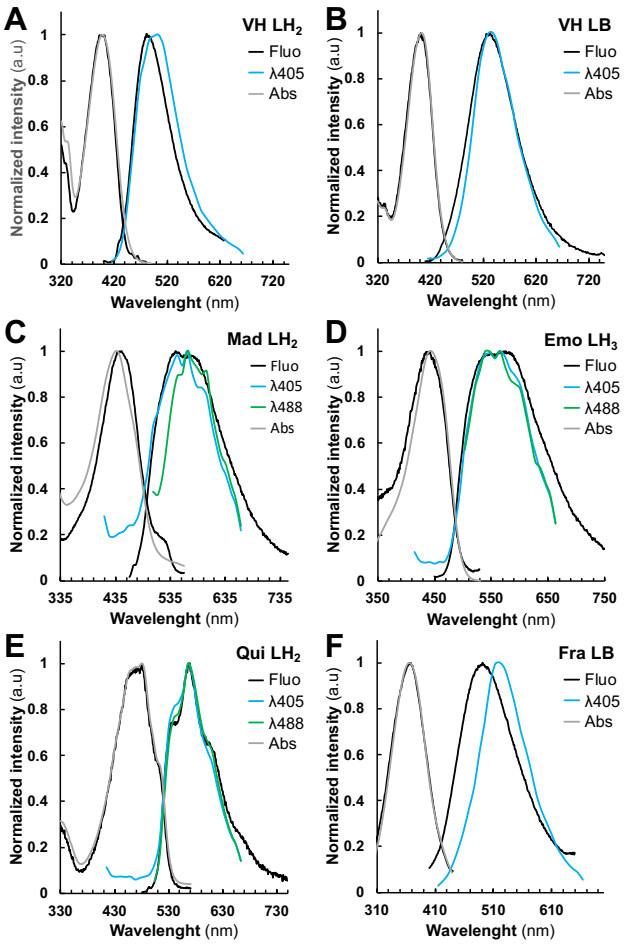

Figure 2. Normalized fluorescence excitation/emission and absorption spectra of studied compounds.
(A) vismione H VH (neutral LH_2 species) and **(B)** (boron complex LB species), **(C)** quinizarin Qui (neutral LH_2 species), **(D)** emodin Emo (neutral LH_3 species), **(E)** madagascine Mad (neutral LH_2 species), **(F)** fraxetin Fra (boron complex LB species) in saline ethanolic solutions. Excitation and emission spectra obtained from the spectrofluorimetric analysis (black), absorption spectra obtained from the UV-Vis. analysis (grey) and SImaging at λ_{405} (blue) and/or λ_{488} (green) settings.

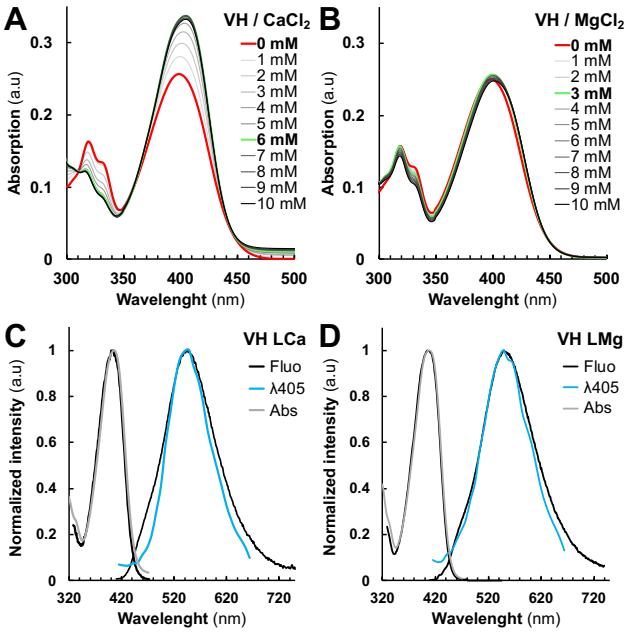

Figure 3. Vismione H VH photophysical properties are influenced by metal cations complexation.
(A-B) Absorption spectra of metal complexes formed by VH with different amount of **(A)** Ca(II) and **(B)** Mg(II) spectra with no complex formed (bold red) and with the highest changes in the absorption spectrum (bold green). Normalized fluorescence (black), absorption (grey) and SImaging spectra of **(C)** VH-Ca and **(D)** VH-Mg complexes at λ_{405} settings.

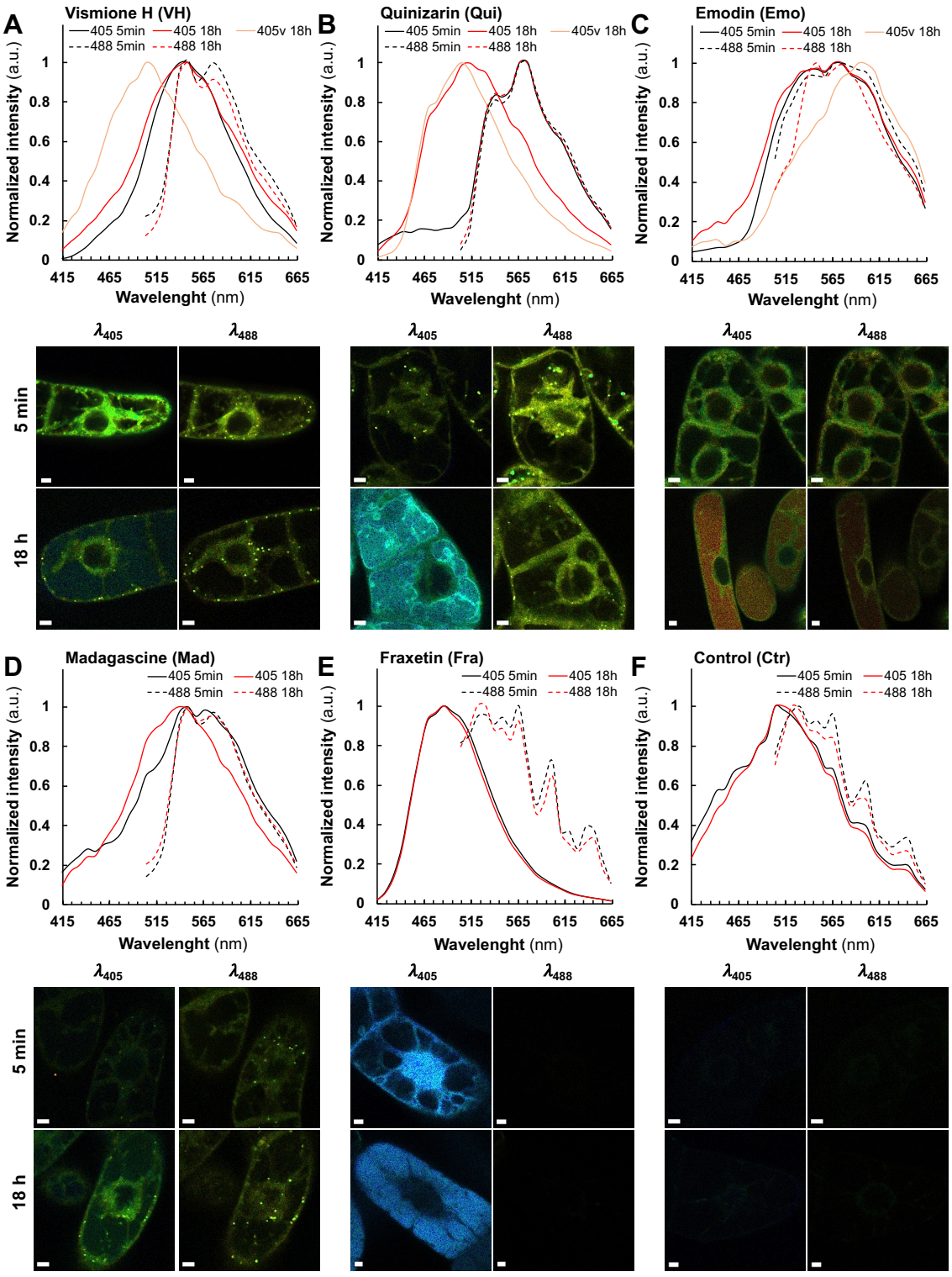
A
Vismione H (VH)
B
Quinizarin (Qui)
C
Emodin (Emo)
D
Madagascine (Mad)
E
Fraxetin (Fra)
F
Control (Ctr)
405 5min
405 18h
405v 18h
488 5min
488 18h
Normalized intensity (a.u.)
Wavelenght (nm)
λ405
λ488
5 min
18 h

Figure 4. Fluorescence spectra and images of BY-2 cells treated by 25 µM of phenolic compounds prior to observation using SImaging.
Normalized fluorescence average spectra and lambda view images from SImaging analysis at λ_{405} (solid line) and λ_{488} (dashed line) of BY-2 cells treated for 5 min and 18 h with 25 µM of **(A)** vismione H, **(B)** quinizarin, **(C)** emodin, **(D)** madagascine, **(E)** fraxetin and **(F)** the negative control without treatment. Spectra observed after 5 min (black), after 18 h (red) and in the vacuole after 18 h (red light). Spectra observed in the primary vacuole at λ_{405} after 18 h are specified with a "v" after the labels if another fluorescence was observed in the cytoplasm. Bars = 20 µm.

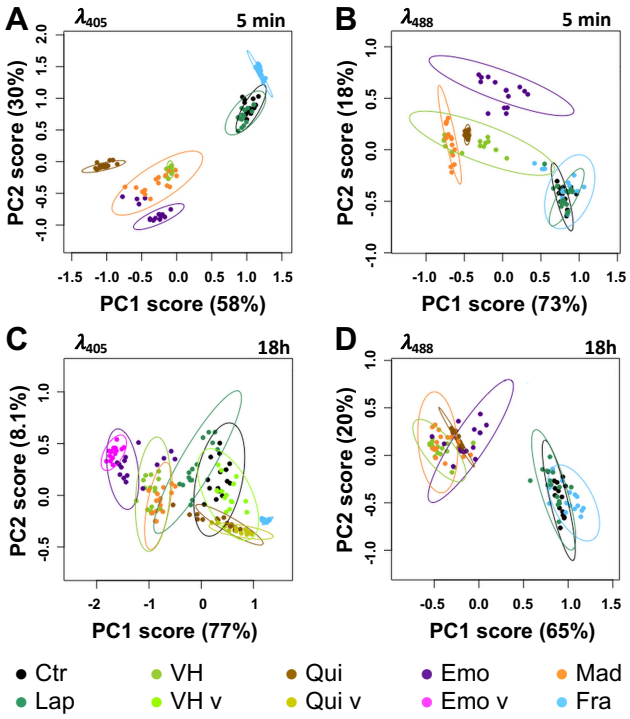

Figure 5. PCA of normalized average spectra obtained by SImaging analysis of BY-2 cells treated or not (Ctr) with 25 µM of phenolic compounds. **(A, B)** Differences observed after 5 min treatments and **(C, D)** 18 h with vismione H VH, madagascine Mad, emodin Emo, quinizarin Qui, fraxetin Fra and lapachol Lap. Spectra observed at λ_{405} **(A, C)** and λ_{488} **(B, D)** in control and treated cells. Spectra found in the primary vacuole at λ_{405} after 18 h are specified with a "v" after the labels if another fluorescence was observed in the cytoplasm. Ellipses are representative of qualitative differences with a $p \leq 0.05$ at the PCA analysis of normalized average spectra.

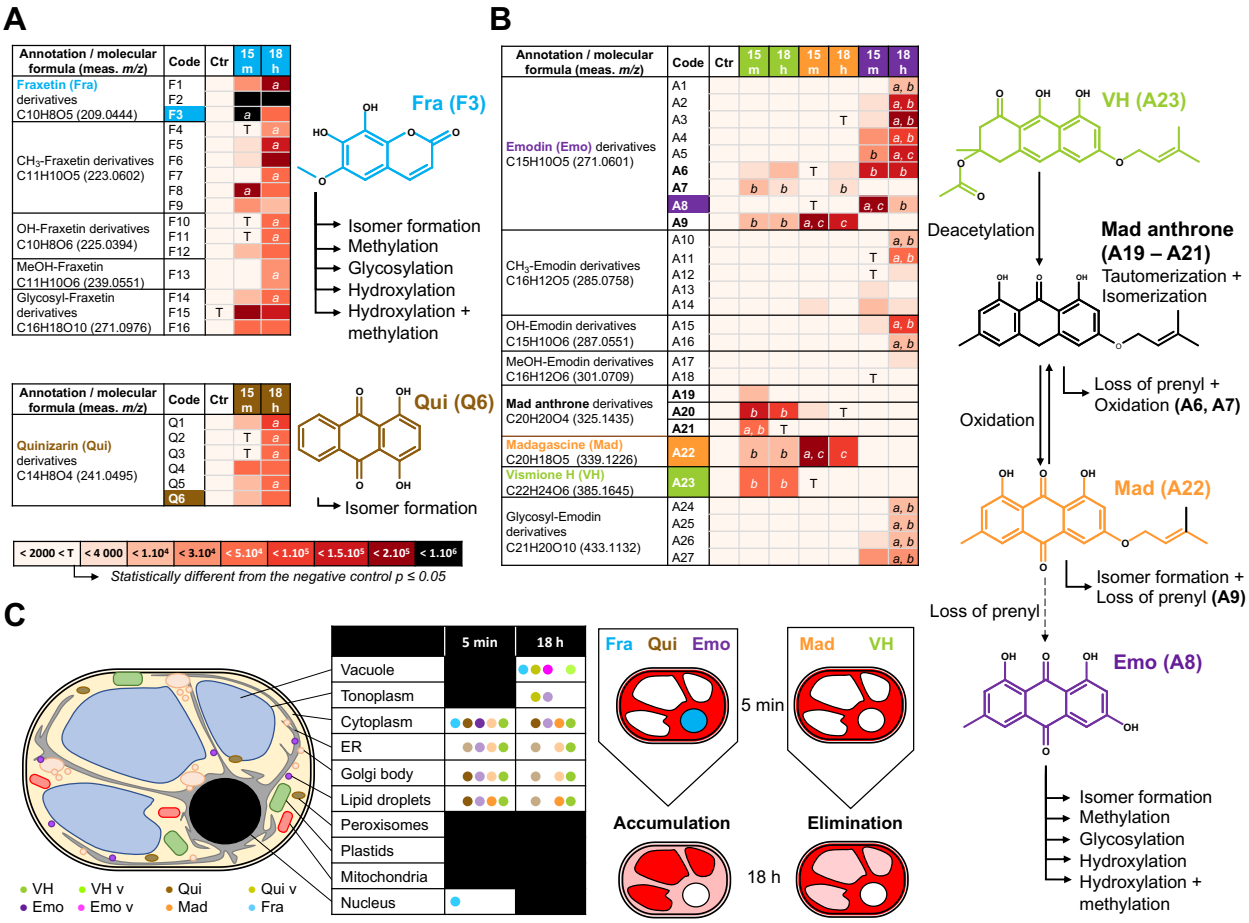

Figure 6. Hypothetical metabolization reactions according to non-targeted analysis of treated BY-2 cells.

m/z of parent and daughter ions from references and related metabolites detected by UPLC-HRMS/MS analysis of methanolic extracts from BY-2 cells treated for 15 min (15 m) and 18 h with **(A)** 50 µM of fraxetin Fra (blue), **(B)** quinizarin Qui (brown) or, **(C)** vismione H VH (green), emodin Emo (purple) and madagascine Mad (orange). meas. *m/z* = measured *mass to charge ratio* of the most intense adduct detected. Proposed reactions such as hydroxylation (+ OH), methylation (+ CH_3), hydroxylation/methylation (+ MeOH), glycosylation (+ Sugar) and loss of prenyl which may occur in the metabolization processes. The arrows indicate hypothetical reactions according to the references (colored label) and 54 annotations absent or with an area below the significant threshold in negative control samples (< 4000). Statistical analysis was performed on area from annotated metabolites (*N*=3) using Levene with Kruskal-Wallis tests followed by a Dunnett's post-hoc test. Significant differences ($p \leq 0.05$) between area of metabolites from BY-2 cells treated 15 min and 18 h (a) or between treatments with anthranoids (b ≠ c). **(D)** Conjuncture of the fluorescence localization in BY-2 subcellular compartments observed by SImaging and the non-targeted metabolomic analysis proposing that Fra, Qui and Emo derivatives accumulate into the vacuole, while not prenylated anthranoids VH and Mad being mostly metabolized into other sub-cellular compartments.

89 **Table 1. Main photophysical characteristics of fluorescent species**

	[C] (μM)	λ_{abs} (nm)	ε (10^4 M^{-1} cm^{-1})	λ_{Ex} (nm)	λ_{Em} (nm)	Φ_F (%)	SI λ_{Em} (nm)
Vismione **H** (LH_2)[a]	2.6	398	1.1	400	481	3.9	503
Vismione **H** (LB)[b]		403	1.40	402	532	31.0	530
Vismione **H** (LNH_4^+)[c]		403	1.93	403	533	23.9	530
Vismione **H-Ca** (LCa)[d]		404	1.36	404	549	19.8	548
Vismione **H-Mg** (LMg)[e]		407	1.40	404	550	18.6	548
Vismione **H-BSA** (LBSA)[f]		404	1.21	404	517	23.5	530
Emodin (LH_3)[a]	5.55	443	1.68	442	575	0.4	565
Madagascine (LH_2)[a]	2.96	437	0.64	446	544	4.8	565
Quinizarin (LH_2)[a]	4.16	480	0.38	479	569	15.1	565
Fraxetin (LB)[b]	4.8	366	1.05	367	492	1.1	521
Fraxetin (LNH_4^+)[c]		399	0.87	382	481	7.7	521
Fraxetin**-BSA** (LBSA)[f]		410	2.04	410	490	8.4	503

The absorption (λ_{abs}), excitation (λ_{Em}) and emission (λ_{Em}) maxima obtained by spectrofluorimetry and SImaging (SI λ_{Em}), the molar extinction coefficient (Ɛ) and quantum yields determined for the pure compounds at different concentration ([C]) in model solutions. EtOH/H_2O 1:1 *v/v*, 0.1 M NaCl with [a] 0.01 M HCl at pH 2, [b] 0.01 M $Na_2B_4O_7$ at pH 10, [c] 0.01 M NH_4HCO_3 at pH 10, [d] 15 mM $CaCl_2$, [e] 15 mM $MgCl_2$, or [f] H_2O containing 300 μM BSA. The errors on ε and Φ_F are estimated to 10%, the errors on λ are estimated to ± 1 nm.

90

91

Parsed Citations

Batchelor-McAuley, C., Dimov, I.B., Aldous, L., and Compton, R.G. (2011). The electrochemistry of quinizarin revealed through its mediated reduction of oxygen. Proc. Natl. Acad. Sci. 108: 19891–19895.
Google Scholar: Author Only Title Only Author and Title

Binzel, M.L., Hess, F.D., Bressan, R.A., and Hasegawa, P.M. (1988). Intracellular Compartmentation of Ions in Salt Adapted Tobacco Cells. Plant Physiol. 86: 607–614.
Google Scholar: Author Only Title Only Author and Title

Cameron, D., Edmonds, J., and Raverty, W. (1976). Oxidation of emodin anthrone and stereochemistry of emodin bianthrone. Aust. J. Chem. 29: 1535.
Google Scholar: Author Only Title Only Author and Title

Carden, D.E., Walker, D.J., Flowers, T.J., and Miller, A.J. (2003). Single-Cell Measurements of the Contributions of Cytosolic Na + and K + to Salt Tolerance. Plant Physiol. 131: 676–683.
Google Scholar: Author Only Title Only Author and Title

Chiang, Y.-M., Szewczyk, E., Davidson, A.D., Entwistle, R., Keller, N.P., Wang, C.C.C., and Oakley, B.R. (2010). Characterization of the Aspergillus nidulans Monodictyphenone Gene Cluster. Appl. Environ. Microbiol. 76: 2067–2074.
Google Scholar: Author Only Title Only Author and Title

Conéjéro, G., Noirot, M., Talamond, P., and Verdeil, J.-L. (2014). Spectral analysis combined with advanced linear unmixing allows for histolocalization of phenolics in leaves of coffee trees. Front. Plant Sci. 5.
Google Scholar: Author Only Title Only Author and Title

Dong, X., Fu, J., Yin, X., Cao, S., Li, X., Lin, L., Huyiligeqi, and Ni, J. (2016). Emodin: A Review of its Pharmacology, Toxicity and Pharmacokinetics: Emodin: Pharmacology, Toxicity and Pharmacokinetics. Phytother. Res. 30: 1207–1218.
Google Scholar: Author Only Title Only Author and Title

Dudev, T. and Lim, C. (2004). Monodentate versus Bidentate Carboxylate Binding in Magnesium and Calcium Proteins: What Are the Basic Principles? J. Phys. Chem. B 108: 4546–4557.
Google Scholar: Author Only Title Only Author and Title

Duval, R., Cottet, K., Blaud, M., Merckx, A., Houzé, S., Grellier, P., Lallemand, M.-C., and Michel, S. (2020). A Photoalkylative Fluorogenic Probe of Guttiferone A for Live Cell Imaging and Proteome Labeling in Plasmodium falciparum. Molecules 25: 5139.
Google Scholar: Author Only Title Only Author and Title

Duval, R. and Duplais, C. (2017). Fluorescent natural products as probes and tracers in biology. Nat. Prod. Rep. 34: 161–193.
Google Scholar: Author Only Title Only Author and Title

Elkazaz, S. and Jones, P.B. (2010). Photochemical Hydroxylation of 1-Methyl-9,10-anthraquinones: Synthesis of 9′-Hydroxyaloesaponarin II. J. Org. Chem. 75: 412–416.
Google Scholar: Author Only Title Only Author and Title

Fain, V.Ya., Zaitsev, B.E., and Ryabov, M.A. (2006). Tautomerism of anthraquinones: V. 1,5-Dihydroxy-9,10-anthraquinone and its substituted derivatives. Russ. J. Org. Chem. 42: 1662–1667.
Google Scholar: Author Only Title Only Author and Title

François, G., Steenackers, T., Assi, L.A., Steglich, W., Lamottke, K., Holenz, J., and Bringmann, G. (1999). Vismione H and structurally related anthranoid compounds of natural and synthetic origin as promising drugs against the human malaria parasite Plasmodium falciparum: structure-activity relationships. Parasitol. Res. 85: 582–588.
Google Scholar: Author Only Title Only Author and Title

Friedman, M. and Jürgens, H.S. (2000). Effect of pH on the Stability of Plant Phenolic Compounds. J. Agric. Food Chem. 48: 2101–2110.
Google Scholar: Author Only Title Only Author and Title

Fujii, T., Mishima, S., Tanaka, N., Kawauchi, O., Kodaira, K., Nishikiori, H., and Kawai, Y. (1997). Absorption and fluorescence spectra of 9-anthrol and its chemical species in solution. Res. Chem. Intermed. 23: 829–839.
Google Scholar: Author Only Title Only Author and Title

Furumoto, T. and Jindai, A. (2008). Isolation and Photoisomerization of a New Anthraquinone from Hairy Root Cultures of Sesamum indicum. Biosci. Biotechnol. Biochem. 72: 2788–2790.
Google Scholar: Author Only Title Only Author and Title

Gallé, J.-B. (2015). Pharmacochimie d'anthranoïdes issus du genre Psorospermum (Hypericaceae): isolement, activités antiparasitaires et synthèse d'analogues structuraux Jean-Baptiste Galle.

Gill, M. (2001). The Biosynthesis of Pigments in Basidiomycetes. Aust. J. Chem. 54: 721.
Google Scholar: Author Only Title Only Author and Title

Giusti, M.M. and Wrolstad, R.E. (2001). Characterization and Measurement of Anthocyanins by UV-Visible Spectroscopy. Curr. Protoc. Food Anal. Chem. 00: F1.2.1-F1.2.13.

Google Scholar: Author Only Title Only Author and Title

Guo, W., Chen, S., Hussain, N., Cong, Y., Liang, Z., and Chen, K. (2015). Magnesium stress signaling in plant: Just a beginning. Plant Signal. Behav. 10: e992287.
Google Scholar: Author Only Title Only Author and Title

Han, Y.-S., Van der Heijden, R., and Verpoorte, R. (2001). Biosynthesis of anthraquinones in cell cultures of the Rubiaceae. Plant Cell Tissue Organ Cult. 67: 201–220.
Google Scholar: Author Only Title Only Author and Title

Hemmerlin, A. and Bach, T.J. (2000). Farnesol-induced cell death and stimulation of 3-hydroxy-3-methylglutaryl-coenzyme A reductase activity in tobacco cv bright yellow-2 cells. Plant Physiol. 123: 1257–1268.
Google Scholar: Author Only Title Only Author and Title

Hepler, P.K. (2005). Calcium: A Central Regulator of Plant Growth and Development. Plant Cell 17: 2142–2155.
Google Scholar: Author Only Title Only Author and Title

Hlasiwetz, H. and Grabowski, A. (1867). Mittheilungen aus dem chemischen Laboratorium in Innsbruck. I. Ueber die Carminsäure; Ann. Chem. Pharm. 141: 329–345.
Google Scholar: Author Only Title Only Author and Title

Kang, S.-H. et al. (2020). Genome-enabled discovery of anthraquinone biosynthesis in Senna tora. Nat. Commun. 11: 5875.
Google Scholar: Author Only Title Only Author and Title

Lefèvre, F., Fourmeau, J., Pottier, M., Baijot, A., Cornet, T., Abadía, J., Álvarez-Fernández, A., and Boutry, M. (2018). The Nicotiana tabacum ABC transporter NtPDR3 secretes O-methylated coumarins in response to iron deficiency. J. Exp. Bot. 69: 4419–4431.
Google Scholar: Author Only Title Only Author and Title

Martinière, A., Bassil, E., Jublanc, E., Alcon, C., Reguera, M., Sentenac, H., Blumwald, E., and Paris, N. (2013). In Vivo Intracellular pH Measurements in Tobacco and Arabidopsis Reveal an Unexpected pH Gradient in the Endomembrane System. Plant Cell 25: 4028–4043.
Google Scholar: Author Only Title Only Author and Title

Mazimba, O., Nana, F., and Singh, G.S. (2013). Xanthones and Anthranoids from the Medicinal Plants of Africa. In Medicinal Plant Research in Africa, V. Kuete, ed (Elsevier), pp. 393–434.
Google Scholar: Author Only Title Only Author and Title

Nagata, T., Nemoto, Y., and Hasezawa, S. (1992). Tobacco BY-2 Cell Line as the "HeLa" Cell in the Cell Biology of Higher Plants. In International Review of Cytology (Elsevier), pp. 1–30.
Google Scholar: Author Only Title Only Author and Title

Osoba, O.A. and Roberts, M.F. (1994). Methyltransferase activity in Ailanthus altissima cell suspension cultures. Plant Cell Rep. 13: 277–281.
Google Scholar: Author Only Title Only Author and Title

Robe, K. et al. (2021). Coumarin accumulation and trafficking in Arabidopsis thaliana : a complex and dynamic process. New Phytol. 229: 2062–2079.
Google Scholar: Author Only Title Only Author and Title

Rossi, S., Tabolacci, C., Lentini, A., Provenzano, B., Carlomosti, F., Frezzotti, S., and Beninati, S. (2010). Anthraquinones danthron and quinizarin exert antiproliferative and antimetastatic activity on murine B16-F10 melanoma cells. Anticancer Res. 30: 445–449.
Google Scholar: Author Only Title Only Author and Title

Sedaira, H., Idriss, K.A., Seleim, M.M., and Abdel-Aziz, M.S. (1998). Use of Quinizarin as a Spectrophotometric Reagent for MgO Content Analysis of Portland Cement and Cement Clinker. Monatshefte Für Chem. Chem. Mon. 129: 49–58.
Google Scholar: Author Only Title Only Author and Title

Shen, J., Zeng, Y., Zhuang, X., Sun, L., Yao, X., Pimpl, P., and Jiang, L. (2013). Organelle pH in the Arabidopsis Endomembrane System. Mol. Plant 6: 1419–1437.
Google Scholar: Author Only Title Only Author and Title

Srinivas, G., Babykutty, S., Sathiadevan, P.P., and Srinivas, P. (2007). Molecular mechanism of emodin action: Transition from laxative ingredient to an antitumor agent. Med. Res. Rev. 27: 591–608.
Google Scholar: Author Only Title Only Author and Title

Stringlis, I.A., de Jonge, R., and Pieterse, C.M.J. (2019). The Age of Coumarins in Plant–Microbe Interactions. Plant Cell Physiol. 60: 1405–1419.
Google Scholar: Author Only Title Only Author and Title

Talamond, P., Verdeil, J.-L., and Conéjéro, G. (2015). Secondary Metabolite Localization by Autofluorescence in Living Plant Cells. Molecules 20: 5024–5037.
Google Scholar: Author Only Title Only Author and Title

Tissier, A., Ziegler, J., and Vogt, T. (2014). Specialized Plant Metabolites: Diversity and Biosynthesis. In Ecological Biochemistry, G.-J.

Krauss and D.H. Nies, eds (Wiley-VCH Verlag GmbH & Co. KGaA: Weinheim, Germany), pp. 14–37.
Google Scholar: Author Only Title Only Author and Title

Tsai, H.-H., Rodríguez-Celma, J., Lan, P., Wu, Y.-C., Vélez-Bermúdez, I.C., and Schmidt, W. (2018). Scopoletin 8-Hydroxylase-Mediated Fraxetin Production Is Crucial for Iron Mobilization. Plant Physiol. 177: 194–207.
Google Scholar: Author Only Title Only Author and Title

Verebova, V., Belej, D., Joniova, J., Jurasekova, Z., Miskovsky, P., Kozar, T., Horvath, D., Stanicova, J., and Huntosova, V. (2016). Deeper insights into the drug defense of glioma cells against hydrophobic molecules. Int. J. Pharm. 503: 56–67.
Google Scholar: Author Only Title Only Author and Title

Villette, C., Maurer, L., Wanko, A., and Heintz, D. (2019). Xenobiotics metabolization in Salix alba leaves uncovered by mass spectrometry imaging. Metabolomics 15: 122.
Google Scholar: Author Only Title Only Author and Title

Villette, C., Zumsteg, J., Schaller, H., and Heintz, D. (2018). Non-targeted metabolic profiling of BW312 Hordeum vulgare semi dwarf mutant using UHPLC coupled to QTOF high resolution mass spectrometry. Sci. Rep. 8.
Google Scholar: Author Only Title Only Author and Title

Waters, B.M. (2011). Moving magnesium in plant cells: Commentary. New Phytol. 190: 510–513.
Google Scholar: Author Only Title Only Author and Title

Yamamoto, H., Tabata, M., and Leistner, E. (1987). Cytological changes associated with induction of anthraquinone synthesis in photoautotrophic cell suspension cultures of Morinda lucida. Plant Cell Rep. 6: 187–190.
Google Scholar: Author Only Title Only Author and Title